NMR spin diffusion measurements in disordered polymers: Insights and limitations

Eric G. Sorte,[1] Amalie L. Frischknecht,[2] and Todd M. Alam[1,*]

[1]*Department of Organic Materials Science, Sandia National Laboratories, Albuquerque, New Mexico 87185 USA*

[2]*Center for Integrated Nanotechnologies, Sandia National Laboratories, Albuquerque, New Mexico 87185, USA*

(Received 22 January 2019; published 19 April 2019)

Nuclear magnetic resonance (NMR) spin diffusion measurements have been widely used to estimate domain sizes in a variety of polymer materials. In cases where the domains are well-described as regular, repeating structures (e.g., lamellar, cylindrical channels, monodispersed spherical domains), the domain sizes estimated from NMR spin diffusion experiments agree with the characteristic length scales obtained from small-angle x-ray scattering and microscopy. In our laboratory, recent NMR spin diffusion experiments for hydrated sulfonated Diels Alder poly(phenylene) (SDAPP) polymer membranes have revealed that assuming a simple structural model can often misrepresent or overestimate the domain size in situations where more complex and disordered morphologies exist. Molecular dynamics simulations of the SDAPP membranes predict a complex heterogeneous hydrophilic domain structure that varies with the degree of sulfonation and hydration and is not readily represented by a simple repeating domain structure. This heterogeneous morphology results in NMR-measured domain sizes that disagree with length scales estimated from the ionomer peak in scattering experiments. Here we present numerical NMR spin diffusion simulations that show how structural disorder in the form of domain size distributions or domain clustering can significantly impact the spin diffusion analysis and estimated domain sizes. Simulations of NMR spin diffusion with differing domain size distributions and domain clustering are used to identify the impact of the heterogeneous domain structure and highlight the limitations of using NMR spin diffusion techniques for irregular structures.

DOI: 10.1103/PhysRevMaterials.3.045602

I. INTRODUCTION

Traditional scattering or microscopy measurements can prove challenging to interpret when characterizing disordered or amorphous solids. In the case of heterogeneous polymers, the size and morphology of phase-separated polymer domains can dictate material properties such as ionic conductivity and mechanical strength [1–5], and are thus important to measure and control. These phase-separated regions or domains may range from the micro- to the nanoscale, further complicating complete characterization. Nuclear magnetic resonance (NMR) spin diffusion is one technique that has been used to characterize morphology in disordered heterogeneous solids [6–14]. During NMR spin diffusion experiments, nuclear spin magnetization in regions/domains of interest are filtered by specifically designed NMR pulse sequences to create spin polarization gradients within the sample, which then reequilibrate via "spin diffusion". This diffusion of spin magnetization relies on the through-space dipolar coupling between nuclei.

In polymers exhibiting well-organized structures, such as lamellar or repeating cylindrical domains, NMR spin diffusion experiments measure domain sizes that agree well with small-angle x-ray scattering (SAXS) and microscopy measurements [7,15–17]. The dimensionality of the spin diffusion process [one-dimensional (1D) for lamellar structures, 2D for cylindrical rod-like domains, and 3D for dispersed domains] is a dominant feature in the spin diffusion behavior [7,18], and is usually determined from other experimental evidence. In disordered or poorly defined polymer morphologies, however, it has been noted that NMR spin diffusion measurements analyzed assuming a simple structural model often yield domain sizes which are larger than those implied by transmission electron microscopy (TEM), scanning electron microscopy or SAXS [16,19–21]. In experiments where this discrepancy has been noted, authors have attributed the conflicting data to inaccuracies in the TEM measurements [20], to the lack of sensitivity in the x-ray diffraction analysis [21], to disorder of domains, to distribution of domain sizes [19], or to errors in the NMR spin diffusion measurements themselves [16]. In some instances where the domain structure is well characterized by scattering techniques, the measured differences have also been used to adjust the NMR spin diffusion rate constant [22]. While the impact of disorder in the polymer morphology was realized early on in the discussion of NMR spin diffusion experiments [19], it has not been routinely incorporated into the spin diffusion analysis. More recently, examples of NMR spin diffusion studies for polymer materials containing domain size distributions [11], or "nontrivial" arrangements and interfaces with differential dynamics have been reported, including suggestions that the impact of disordered heterogeneous polymer structures on NMR spin diffusion experiments needs to be further explored [23–26].

Recently, we have reported extensive characterization of a series of sulfonated Diels-Alder poly(phenylene) (SDAPP) polymer membranes (see Scheme 1) [27]. When hydrated, the

*Author to whom correspondence should be addressed: tmalam@sandia.gov

SDAPP polymers phase separate into nanodomains containing the hydrophobic aromatic polyphenylene backbone and domains containing the hydrophilic sulfonic acid and associated water. In our study, the characteristic length scale (d^*) of the polymer domains for a range of ion exchange capacities (IECs) was estimated from experimental SAXS structure factors $S(q)$ or from the molecular-dynamics (MD)-predicted $S(q)$ [27]. The reported d^* range from 2 to 3 nm, varying with the SDAPP hydration and sulfonation levels. This is consistent with the 2–4 nm d^* recently reported for a similar SDAPP material [28]. In a related study, it was found that using these MD-predicted SDAPP polymer structures yielded NMR spin diffusion magnetization recovery curves that agreed well with experimental NMR results [18]. However, when the NMR spin diffusion behavior was analyzed assuming simple well-structured geometric models, the estimated domain sizes (d^{NMR}) were up to five times larger ($\sim$15 nm at the highest levels of sulfonation and hydration) than the d^* obtained from SAXS and MD simulations. Inspection of the MD-predicted structures for the SDAPP polymer reveal that the hydrophilic domains are not simple well-organized structures, but have heterogeneous morphologies with distributions of both domain sizes and shapes [29]. In this work, we present numerical simulations to identify the basis for the discrepancy in length scales between NMR, the MD simulations and the SAXS data. The role of domain size distribution and hydrophilic domain clustering on the NMR spin diffusion behavior will be discussed and used to place boundaries on the applicability of NMR spin diffusion measurements when studying disordered materials such as heterogeneous nanoscale polymers, nanoscale composites, layered materials, and polymer modified nanoparticles.

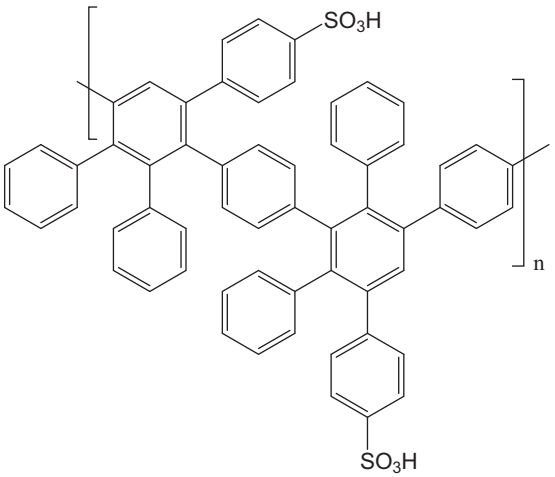

Scheme 1. Monomer structure for the SDAPP polymer containing two sulfonic acid groups ($S = 2$) per monomer repeat unit.

II. MATERIALS AND METHODS

NMR Spectroscopy. Experimental details for the static and magic angle spinning (MAS) NMR spin diffusion studies have been presented previously [18]. In summary, the solid state ^{1}H MAS NMR was performed on a Bruker Avance III spectrometer operating at a Larmor frequency of 600.1 MHz using a 2.5-mm MAS probe spinning at 20 kHz or under static (nonspinning) conditions, with a 4-s recycle delay and a 100-kHz ^{1}H rf field. Double-quantum (DQ) filtered pulse sequences [18,21,30–33] were used to retain magnetization in the rigid aromatic polymer phase while suppressing magnetization in the mobile hydrophilic phase, followed by diffusion of the magnetization via the homonuclear ^{1}H^{-1}H homonuclear dipolar coupling back into the hydrophilic domain (See Fig. S6, in the Supplemental Material [34]). The signal intensity was measured for both the hydrophilic and hydrophobic domains following a spin diffusion period (t_{SD}) to produce the experimental NMR spin diffusion recovery curves [Figs. 1(b) and 1(c)]. For the static DQ-filtered spin diffusion experiments a standard 5-pulse sequence was used for the DQ excitation and reconversion period, with π refocusing pulses incorporated to reduce frequency offset and chemical shift effects [35–37]. The DQ evolution period was fixed to 2 μs while incrementing the spin diffusion period t_{SD}. The DQ-filtered ^{1}H MAS NMR spin diffusion experiments used a rotor-synchronized back-to-back excitation/conversion pulse sequence to suppress the hydrophilic domain ^{1}H magnetization [14], with the rotor-synchronized excitation time being set to $N = 2$ rotor cycles, followed by a variable spin diffusion period t_{SD}. It has been noted that the hydrophilic domains could contain partially ordered water that may give rise to nonzero DQ intensity. For these ordered water species the magnitude of the residual dipolar coupling is expected to be weak. Under the short DQ excitation/reconversion periods utilized (2 μs for static and 2 rotor cycles for MAS), the signal intensity in the hydrophilic domain immediately following the DQ filtering was not readily detected and was therefore ignored during subsequent analysis. For both pulse sequences the DQ selection was obtained using a 4-step phase cycle of the carrier phase during the excitation period combined with receiver phase inversion on alternating scans. Between 64 and 256 scan averages were required for each spin diffusion time depending on the sample and hydration level. The nominal sample temperature was 298 K for the static experiments and 311 K under MAS conditions after correction for frictional heating.

Simulations. The simulation program NMR_DIFF_SIM [18] was used to predict magnetization behavior through numerical solutions of the continuum diffusion equation on a discretized lattice for any proposed domain structure assuming periodic boundary conditions. The (continuum) time evolution of the spin magnetization is given by [18]

$$\frac{\partial m(\vec{r},t)}{\partial t} = \nabla \cdot [D(\vec{r})\,\nabla m(\vec{r},t)], \tag{1}$$

which is discretized for the numerical evaluation as

$$\frac{\partial m(\vec{r},t)}{\partial t} = \frac{\partial}{\partial x}\left\{D(\vec{r})\,\frac{\partial}{\partial x}m(\vec{r},t)\right\} + \frac{\partial}{\partial y}\left\{D(\vec{r})\,\frac{\partial}{\partial y}m(\vec{r},t)\right\} + \frac{\partial}{\partial z}\left\{D(\vec{r})\,\frac{\partial}{\partial z}m(\vec{r},t)\right\}, \tag{2}$$

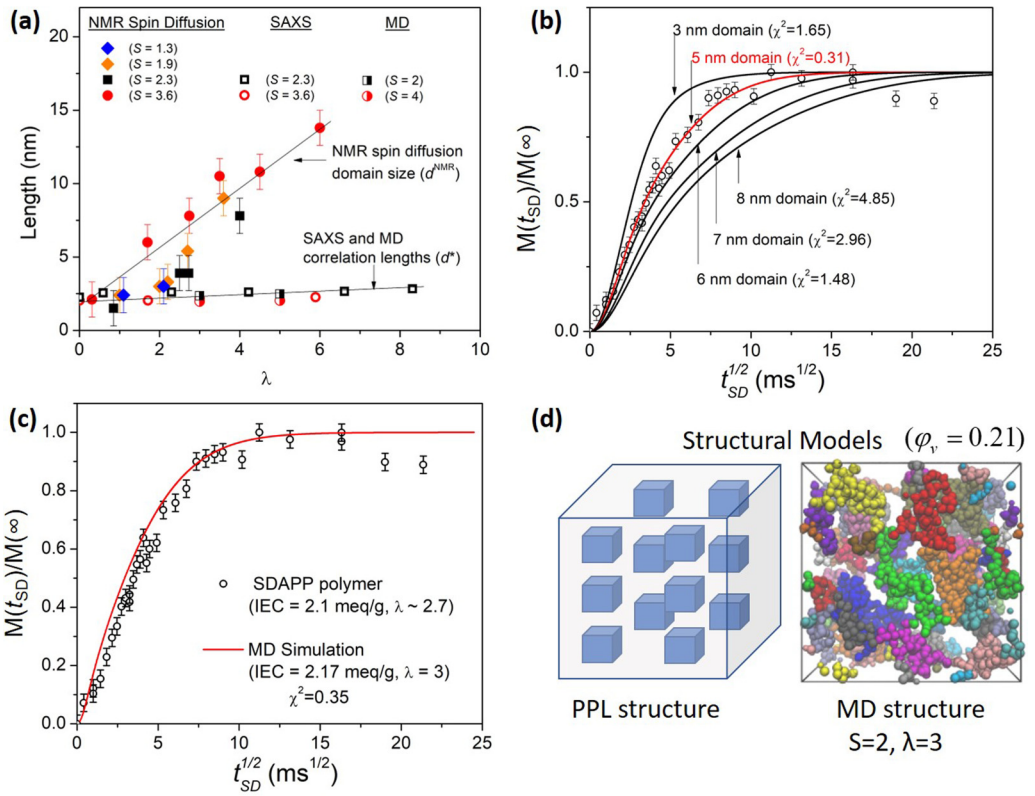

FIG. 1. (a) Characteristic length scale d^{NMR} and d^* for a series of SDAPP polymer membranes as a function of hydration (λ) with different *sulfonation levels* (S): d^* was obtained from SAXS (open symbols) and MD simulation (half-filled symbols) structure factors, while d^{NMR} was obtained from NMR spin diffusion experiments (solid symbols). Solid lines are provided as a visual guide. (b) Simulations of NMR spin diffusion recovery curves using the normalized signal intensity $[M(t_{SD})/M(\infty)]$ obtained for a PPL model [Fig. 1(d)] with different domain sizes for the experimental SDAPP membrane with IEC = 2.1 λ = 2.7. The best fit for a hydrophilic domain size of 5 nm is shown (red line) along with the experimental data (open circles). (c) Normalized NMR spin diffusion signal intensity (red line) using the MD-predicted structure [Fig. 1(d)] as the input geometry compared to the experimental data (open circles). (d) The two structural models used to generate NMR spin diffusion curves; a simple PPL model and the MD structure where only the hydrophilic domains are shown.

where $m(\vec{r}, t)$ is the total magnetization at a specific point in space and time and $D(\vec{r})$ is the spatially dependent diffusion constant.

For the simulations presented here, the spin diffusion constants in the hydrophobic domain (aromatic polymer backbone, domain **A**) were defined as $D_A = 0.2\,nm^2/ms$ and for the hydrophilic polymer domain (sulfonic acid + water, domain **B**) as $D_B = 0.01\,nm^2/ms$ [18]. No intermediate interface regions were employed for the current simulations. In general the spin diffusion rates are a function of the hydration level (λ = water molecules per sulfonic acid), IEC, temperature, and MAS spin rate [18]. To address the role of structural disorder, simulations for a single example of the SDAPP polymer are discussed. Specific results presented here are for a SDAPP membrane with an IEC = 2.10 meq/g, or roughly $S = 1.9$ (where S equals the number of sulfonic acid groups per polymer repeat unit), a λ = 3 hydration level (λ = number of water or hydroniums/sulfonic acid), and a hydrophilic volume fraction of $\varphi_B = 0.21$ [18,29]. For all the simulations described, D_A, D_B, and φ_B were fixed to allow the impact of changes in the polymer disorder to be clearly distinguished. These results were compared to the data from SAXS and the MD simulations described previously [18,27,29].

III. RESULTS AND DISCUSSION

Evaluation of the experimental NMR spin diffusion magnetization recovery curves to obtain the domain size d^{NMR} requires a structural model as input. For the majority of reported NMR spin diffusion studies, a simple well-structured geometrical model has been employed. Ideally, the choice of the diffusion dimensionality and the domain structure for the model is motivated by other characterization data available for that material (e.g., SAXS, microscopy or computational studies). Examples of simple models used to analyze NMR spin diffusion in polymers include domains that are lamellar or sheet-like (1D diffusion), cylindrical channels or tube-like domains (2D diffusion), or regularly spaced isolated dispersed domains (3D diffusion). The domain size in these models then corresponds to the thickness of the lamellar domain, the diameter of the cylindrical channel, or the diameter of the isolated dispersed domain.

Figure 1(a) shows the hydrophilic domain size d^{NMR} obtained from NMR spin diffusion measurements (solid symbols) assuming a simple nanodispersed 3D diffusion model with a single domain size for a series of SDAPP membranes with different IEC values and hydration levels. In these membranes d^{NMR} grows steadily with increasing λ (~2 nm/λ), and

with the variation of d^{NMR} being essentially independent of IEC. This change in hydrophilic domain size with hydration has been observed both in Nafion [38,39] as well as other hydrocarbon polymers [5]. For example, in related (but not identical) sulfonated random copolymers, isolated hydrophilic domain sizes are in the range of 4–6 nm (using scanning transmission electron microscopy (STEM), Watanabe and coworkers [40]), 12–15 nm (TEM, Lee and coworkers [41]), 10–12 nm (TEM, Wang and coworkers [3]), 5–15 nm (using atomic force microscopy (AFM), Ma and coworkers [42]), 5–10 nm (STEM, Miyatake and coworkers [2]), and as large as 25 nm (AFM, Kim and coworkers [43]). This range of domain domain sizes is like those predicted for SDAPP by NMR spin diffusion but are much larger than the reported domain sizes for Nafion at comparable hydration levels.

To estimate the hydrophilic domain size, the diameter of the dispersed domains (3D diffusional model) was varied until a minimum in the χ-squared error between the experimental and simulated data is obtained as shown in Fig. 1(b). Structures with smaller hydrophilic domains have NMR spin magnetization recovery curves that rapidly approach the equilibrium magnetization, while larger domains lead to slower recovery curves. For the domain size measurements in Figs. 1(a) and 1(b), a perfect periodic lattice (PPL) model was used [see Fig. 1(d)], where the hydrophilic domains are dispersed homogeneously on an ordered lattice throughout the polymer.

The NMR spin diffusion results can be compared to the correlation lengths d^* estimated from MD and SAXS data [27], which are calculated from the wavenumber q of the ionomer peak maximum q_{max} observed in the structure factor $S(q)$ using [44]

$$d^* = \frac{2\pi}{q_{max}}. \tag{3}$$

Figure 1(a) compares d^{NMR} with d^* predicted for SDAPP from the MD calculated $S(q)$ (half-filled symbols) and the experimental SAXS $S(q)$ (open symbols) as a function of λ and IEC. The MD and SAXS characteristic length scales d^* range between 2 and 3 nm and are related to the average hydrophilic center-of-mass (COM) to COM distances, with d^* increasing with hydration. Note that the hydrophilic domain size, while not determined from SAXS, is necessarily smaller than the distance between the hydrophilic domains, so d^* serves as an upper bound on the average hydrophilic domain sizes. Incidentally, this range of measured and predicted d^* are similar to the hydrophilic domain spacings measured in Nafion over a similar hydration range [45,46].

Interestingly, while the MD-derived correlation distances are consistent with the SAXS measurements, the NMR spin diffusion-determined d^{NMR} (assuming a simple 3D PPL model) are significantly larger for all S levels, and the discrepancy increases with increasing hydration (d^{NMR} ranging between 2 and 15 nm). It is often true that SAXS correlation lengths do not have a straightforward interpretation [39,46]. The scattering curves are typically fit assuming a structural model, particularly the broad SAXS ionomer peaks observed here for the SDAPP membranes [27]. However as noted above, the correlation lengths obtained from the MD-simulated $S(q)$ agree with the SAXS $S(q)$ derived correlation lengths. We have used real-space imaging from the MD simulations to show that the ionomer peak correlation lengths results from interaggregate scattering (or from scattering between different pieces of long, extended aggregates). For low hydration where the hydrophilic domains are relatively compact and not percolated, the correlation length is the distance between centers of mass of the hydrophilic domains [27].

However, when the MD-calculated structure [Fig. 1(d)] is used as the input model for the NMR spin diffusion simulations instead of assuming a simple 3D nanodispersed domain PPL model, the predicted spin magnetization recovery curve agrees well with the experimental data [Fig. 1(c)]. The question therefore arises: Why are the NMR spin diffusion-measured domain sizes d^{NMR} obtained assuming a PPL model so dramatically different from the d^* derived from SAXS and MD, while clearly the NMR spin diffusion recovery curve agrees when the MD-calculated structure is directly used as the input model?

The choice of the geometric models chosen as input structures for NMR spin diffusion studies is ideally motivated by other experimental characterization. In the case of SDAPP, however, we have no definitive experimental analysis to support any proposed morphology, and initially we chose the simple 3D PPL model for the NMR spin diffusion analysis. Comparison of the PPL model to the MD-predicted hydrophilic cluster morphology [Fig. 1(d)] suggests there may be significant differences between these models. (We note that here we compare to the MD domain morphology obtained from a density-based clustering algorithm, as described in Ref. [29]). One obvious feature in the MD-calculated morphology is an absence of periodicity, with the hydrophilic domains not being regularly spaced. In addition, the domain shapes are irregular (nonspherical and have a distribution of domain sizes; see Fig. 6 of Ref. [29]). We propose that such disordered morphologies may play a role in the domain-size-measurement discrepancy observed in Fig. 1(a), and the effects of such disorder on NMR spin diffusion measurements will be the focus of the discussion.

NMR Spin Diffusion and Structural Disorder. The impact of structural disorder on experimental NMR spin diffusion measurements has not been extensively addressed. Previous authors have explored the effects of domain size distributions, vacancies, or positional disorder using analytical solutions to the diffusion equation [11,19,47]. Several of these disordered morphology types derived from a PPL model are illustrated in Fig. 2. Cheung reported that orientational disorder [Fig. 2(c)] did not affect the NMR spin diffusion behavior because the surface to volume ratio (S/V) and the average distance between the hydrophilic domains remains unchanged. We know that the initial time portion of the NMR magnetization recovery for the hydrophilic domain $M_B(t_{SD})$ is directly proportional to S/V (also known as the initial rate approximation) and is described by [7,18]

$$\frac{M_B(t_{SD})}{M_B(t_{SD}\to\infty)} \approx \frac{S}{V_{total}}\sqrt{t_{SD}}\frac{2}{\sqrt{\pi}}\left(\frac{\rho_{HA}\phi_A+\rho_{HB}\phi_B}{\phi_A\phi_B}\right) \times\left[\frac{\sqrt{D_AD_B}}{\rho_{HA}\sqrt{D_A}+\rho_{HB}\sqrt{D_B}}\right]-O(\sqrt{t_{SD}}^2), \tag{4}$$

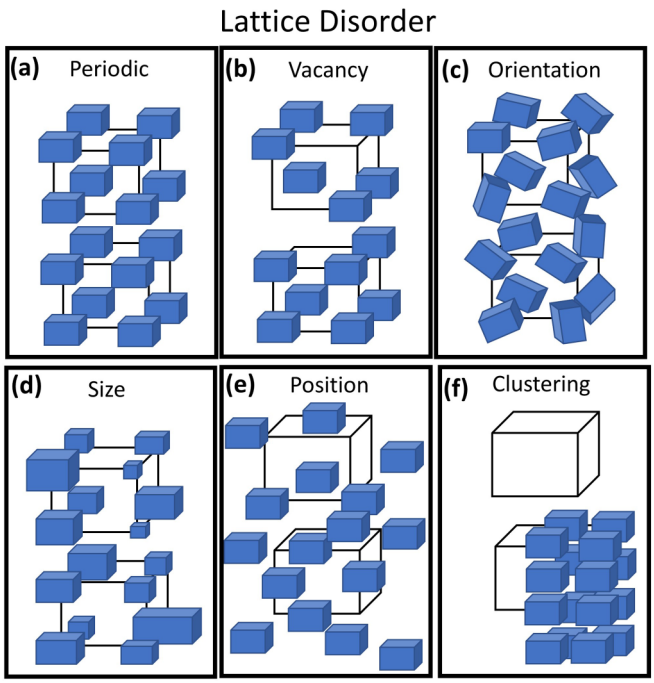

FIG. 2. Illustrations of some possible types of polymer domain structure disorder in comparison to the PPL. The presence of (b) vacancies, (c) orientational disorder, (d) a distribution in domain sizes, (e) positional disorder, or (f) domain clustering are all manifestations of adding disorder starting from well-structured periodic domains.

where V_{total} is the total volume, S is the hydrophilic domain surface area, ρ_{HA}, ρ_{HB} are the proton densities, ϕ_A, ϕ_B are the volume fractions, and D_A, D_B are the spin diffusion constants for the **A** and **B** domains, while the term $O(\sqrt{t_{SD}}^2)$ denotes terms that are quadratic in $\sqrt{t_{SD}}$. The initial linear portion of these recovery curves are directly proportional to S/V_{total}, which can be related to the domain size d^{NMR} for dimensionality ε by

$$d^{NMR} = 2\varepsilon\phi_B \frac{V_{total}}{S}. \quad (5)$$

If S/V, ε, and ϕ are the same for a proposed structure then the initial buildup of the spin magnetization will be equivalent. At longer spin diffusion periods ($\sqrt{t_{SD}}$) the magnetization recovery curves [Eq. (4)] can deviate significantly from this initial linear approximation due to the specifics of the domain morphology including interfaces, domain size distributions, and heterogeneity of the domain locations (e.g., disorder and clustering).

Cheung reported a power-law effect on the spin magnetization recovery curves (i.e., longer recovery times) for structures containing vacancy disorder [Fig. 2(b)] or large distributions of domain size [Fig. 2(d)] [19,47]. He showed that with sufficient disorder, the domain form factors start to include increasingly lower values of the wave vectors q, which cancel in the case of the PPL model. Inclusion of those long wave vectors, which control the long-time behavior of the spin diffusion curve, causes the slower magnetization recovery. This power-law behavior can lead to an overestimation of the average domain size if one models the magnetization recovery curve assuming a simple 3D PPL model (where the domain sizes are constant). For SDAPP membranes the morphology is argued to be very complex and heterogeneous, and not well-described by a regular or periodic structure, for which analytical solutions to the diffusion equation quickly become intractable. Instead, we address the role of different types of disorder through numerical simulations using the NMR_DIFF_SIM program [18]. For this study, we chose to highlight the effects of domain size distributions and of domain clustering (i.e., heterogeneous variations in the spatial arrangement of identically sized domains) on the magnetization recovery, as these are relevant structural motifs in PEMs. The role of vacancies is not discussed here as this disorder produces a change in the volume fraction ϕ_B (a parameter we wanted to keep constant for the simulations), but the behavior of the resulting recovery curves is closely related to significant heterogeneous positional disorder.

Distributions in Domain Sizes. One difference between the MD-predicted SDAPP morphology and the 3D PPL structural model [Fig. 1(d)] is the distribution of domain sizes present in the MD structure. For example, see Fig. 6 of Ref. [29], which shows the distribution in the radius of gyration for the different hydrophilic domains as a function of sulfonation and hydration. We simulated domain size distributions by integrating the recovery of the NMR spin magnetization for different monodispersed domain sizes $M(t_{SD}, d^{NMR})$ [individual spin magnetization recovery curves shown in Fig. 1(b)], with the response for each domain size weighted by the probability distribution function $P(d^{NMR})$

$$M(t_{SD}) = \int P(d^{NMR}) M(t_{SD}, d^{NMR})\, d(d^{NMR}). \quad (6)$$

Here we have assumed that the experimental NMR signal includes the response from different volumes of the polymer where a given domain size dominates the spin magnetization recovery curve. $P(d^{NMR})$ could be described by many different functional forms including Gaussian, Poisson, and β distributions if they are physically realistic in describing the domain structure. It is also possible to iteratively fit the probability distribution coefficients to minimize the difference between the experimental and simulated NMR spin magnetization recovery curves $M(t_{SD})$ to directly obtain the distribution $P(d^{NMR})$. This method has been previously successfully implemented [11], but the uniqueness of the resulting distributions has not been fully evaluated. We explore the impact of varying domain sizes assuming a Gaussian distribution

$$P(d^{NMR}) = \frac{1}{\sqrt{2\pi\sigma^2}} \exp[-(d^{NMR} - \mu)^2/2\sigma^2], \quad (7)$$

where μ is the mean domain size and σ is the standard deviation. The NMR spin magnetization recovery curves for $\mu = 5$ nm [the best fit d^{NMR} for a PPL model, Fig. 1(b)] as a function of σ is shown in Fig. 3. As expected for a very small standard deviation in domain sizes ($\sigma = 0.1$ nm) the NMR spin diffusion recovery curve (dashed red line) is equivalent to the $d^{NMR} = 5$ nm recovery curve in a PPL model (black solid line). With increasing σ (2 and 5 nm) contributions from the other domain sizes produce NMR spin diffusion recovery curves that approach the equilibrium magnetization

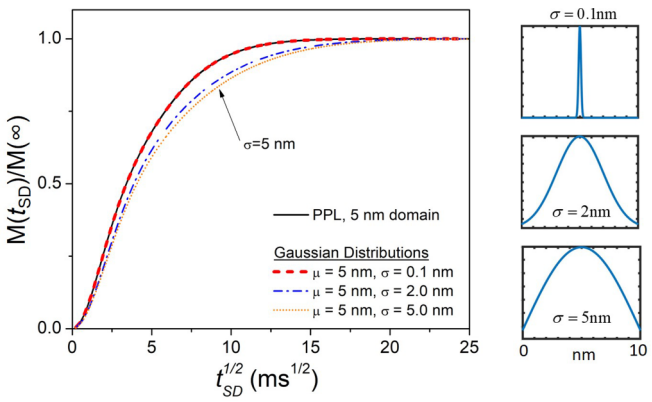

FIG. 3. Simulated NMR spin magnetization recovery curves with a normalized signal intensity $[M(t_{SD})/M(\infty)]$ assuming a PPL structural model with 5-nm domain diameters, and for structures assuming a Gaussian distribution of domain sizes (mean $\mu = 5$ nm) with increasing standard deviations (right) of $\sigma = 0.1$, 2, and 5 nm. Increasing σ leads to a slower spin magnetization recovery.

more slowly, similar to the effect seen for increasing d^{NMR} [Fig. 1(b)]. This means that if the NMR spin magnetization recovery curve was measured and analyzed using only the 3D PPL model with a single domain size, the estimated domain size would be larger than the mean μ domain size in the distribution. The impact of domain size distributions is not dramatic unless the standard deviations are comparable to the domain size. This subtle effect due to the presence of domain size distributions has been noted previously [18]. It should be noted that while the Gaussian $P(d^{NMR})$ is symmetric with respect to d, the response of $M(t_{SD})$ is *not* symmetric with respect to d, with the slower recovery behavior (effective larger d^{NMR}) becoming more important with increasing σ. In the supplemental material, we have explored the effects of other (asymmetric) domain size distributions [48,49] on the spin diffusion recovery curves [34].

Impact of Domain Clustering. Another possible disordering of the polymer morphology away from the simple 3D PPL model structure is heterogeneous clustering of hydrophilic domains, in which the domains are no longer spatially located uniformly throughout the membrane. To explore the impact of clustering, we extended the unit cell of the NMR spin diffusion simulation from a single nanodispersed hydrophilic domain surrounded by the aromatic polymer, to a larger simulation unit cell containing eight hydrophilic domains that can be moved relative to one another [see Fig. 4(a)], while maintaining the same relative volume fraction ϕ_B. For these NMR spin diffusion simulations, the hydrophilic domain sizes were fixed at $d^{NMR} = 5$ nm (linear dimension); this value again was motivated by the PPL model fit in Fig. 1(b).

As shown in Fig. 4(a), the eight hydrophilic domains (of $d^{NMR} = 5$ nm) are located initially $x_0 = 4$ nm apart, with the closest hydrophilic domain COM to COM distance $\mathbf{a} = 9$ nm. The total unit cell has a linear dimension given by $A = 18$ nm, and is governed by the targeted hydrophilic volume fraction φ_B via

$$A = d^{NMR}\left(\frac{N}{\varphi_B}\right)^{1/3}, \tag{8}$$

where N is the number of domains in the primitive unit cell for the simulation. As expected, the calculated NMR spin diffusion recovery curve for this initial eight-domain PPL model configuration is identical to the curve generated by a single domain [Fig. 1(b), $d^{NMR} = 5$ nm] in a proportionally smaller unit cell with the same volume fraction (See Fig. S1, Supplemental Material [34]), and underscores the periodic boundary conditions used in NMR_DIFF_SIM.

To explore the effects of clustering on the NMR spin diffusion curve, the relative proximity of the domains was

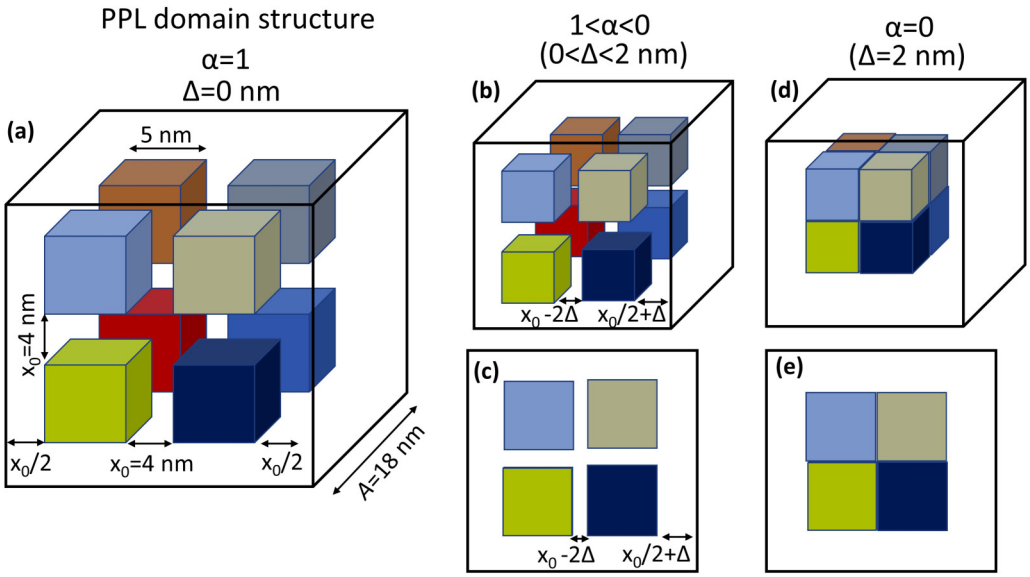

FIG. 4. (a) Initial geometry for simulation of hydrophilic domain clustering with the simulation unit cell containing eight evenly spaced domains for the fixed volume fraction ($\varphi_B = 0.21$). (b) and (c) Visual representation of clustering progress as α decreases (Δ is increased). These structures correspond to the spin diffusion recovery curves in Fig. 6. (b) 3D view, and (c) 2D view of $1 < \alpha < 0$ [intermediate clustering, Eq. (9)]; (d) 3D view, and (e) 2D view of $\alpha = 0$ (full clustering).

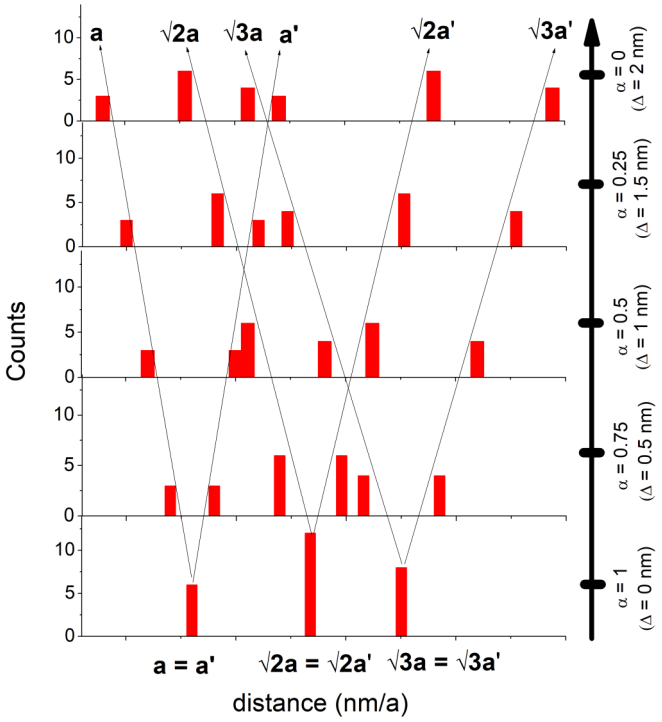

FIG. 5. Distribution of domain-to-domain distances for the structural models in Fig. 4 as a function of the interspacing ratio α [Eq. (9)]. The weighted average distance $\langle d \rangle$ remains unchanged.

reduced as described by the parameter Δ [Fig. 4(b)]; as Δ increases, the eight hydrophilic domains in the unit cell move closer to one another in all three dimensions until a single large domain is obtained (single large cluster). We define the dimensionless ratio

$$\alpha = \frac{x_0 - 2\Delta}{x_0} \tag{9}$$

to describe this clustering. In this example the clustering occurs in a uniform manner, with all the individual domains approaching each other at the same rate. For the initial 3D PPL model structure $\alpha = 1$ [Fig. 4(a)], while for the fully clustered system [single large domain, Fig. 4(d)] $\alpha = 0$. For the structures used in the NMR spin diffusion simulations the domain clustering occurs in the center of the unit cell, but it is known that under periodic boundaries the simulation results are translationally invariant. In addition, clustering of hydrophilic domains in polymer membranes may be expected to be nonuniform (more disorder), and subsequently would require multiple distances to represent the structure.

The initial PPL model structure ($\alpha = 1$) has three unique distances measured from the center of each hydrophilic domain to the center of neighboring domains (Fig. 5). These domain to domain distances split into six unique distances as the clustering proceeds. The end number of unique distances depends on the number of domains in the simulation unit cell. One of the intraunit cell distances (within the primitive unit cell) is parallel to the face of the cluster and described by the lattice parameter **a**, while the related interunit distance (between adjacent unit cells through the periodic boundary conditions) is described by **a**′:

$$\mathbf{a} = \frac{A}{2} - x_0(1-\alpha),$$
$$\mathbf{a}' = \frac{A}{2} + x_0(1-\alpha), \tag{10}$$

where A represents the linear dimension of the simulation unit cell. The hydrophilic domains in the initial PPL model geometry [Fig. 4(a)] have six nearest neighbors linearly along a face, which before clustering ($\alpha = 1$) have COM to COM distances of $\mathbf{a} = \mathbf{a}' = 9$ nm, 12 next-nearest neighbors at the face-diagonal distance of $\sqrt{2}\mathbf{a} = \sqrt{2}\mathbf{a}' = 12.7$ nm, and eight third-nearest-neighbors at the body diagonal distance of $\sqrt{3}\mathbf{a} = \sqrt{3}\mathbf{a}' = 15.6$ nm (Fig. 5, bottom). As the domains begin to cluster, Δ increases and α decreases, with $\mathbf{a} \neq \mathbf{a}'$ as described in Eq. (10). Each of the domain to domain distances split into intraunit and interunit pairs. The discreet distance distribution functions are shown in Fig. 5 as a function of α, with arrows to guide the eye as to which pairs of distances corresponded to which initial values. This figure highlights that domain-to-domain distances can become dispersed with increasing degrees of clustering, even though (for this simulation) the domain sizes are constant. Since the evolution from the initial distribution with decreasing α results in each initial distance splitting into two equal parts that move equal amounts in opposite directions, the weighted average of the distributions

$$\langle d \rangle = \sum_i f_i d_i = \frac{\sum_i d_i n_i}{\sum_i n_i} \tag{11}$$

remains constant at $\langle d \rangle = 12.75$ nm for all values of α. Here, d_i refers to the i^{th} distance, f_i to the relative fraction of this distance and n_i to the number of these distances (In Fig. 5 $\sum n_i = 26$ for all α). This is a very simple clustering model involving individual domains of equal sizes with no size distributions allowing a single parameter α to describe the extent of clustering. For more complex structures the disorder can be described by other methods including the two-point correlation function $g_2(|r_{ab}|)$, the Pearson correlation coefficient or bivariate correlation function $\rho(A, B)$, as further discussed in the Supplemental Material [34]. The NMR spin diffusion simulations (discussed below, Fig. 6) reveal that clustering has a distinct impact on the magnetization behavior even though the average $\langle d \rangle$ remains unchanged. This result reemphasizes that NMR spin diffusion is *not* reflective of an *average* domain-to-domain distance.

The NMR spin magnetization recovery curves for the clustering structural model as a function of α are presented in Fig. 6. We have included the experimental data (open symbols) for the hydrated $S = 1.9$ (IEC = 2.1 meq/g), $\lambda = 3$ SDAPP polymer membrane for comparison [18].

Assuming a simple PPL structural model [Fig. 4(a)] with no clustering ($\alpha = 1$, solid black line), the best fit to the experimental NMR spin diffusion results is with the hydrophilic domain size $d^{\text{NMR}} = 5$ nm [see also Fig. 1(b)]. With increasing degree of hydrophilic domain clustering (decreasing α) the spin magnetization recovery curves take longer to reach equilibrium, which is the same effect of increasing domain size. In the limit of complete clustering of the individual

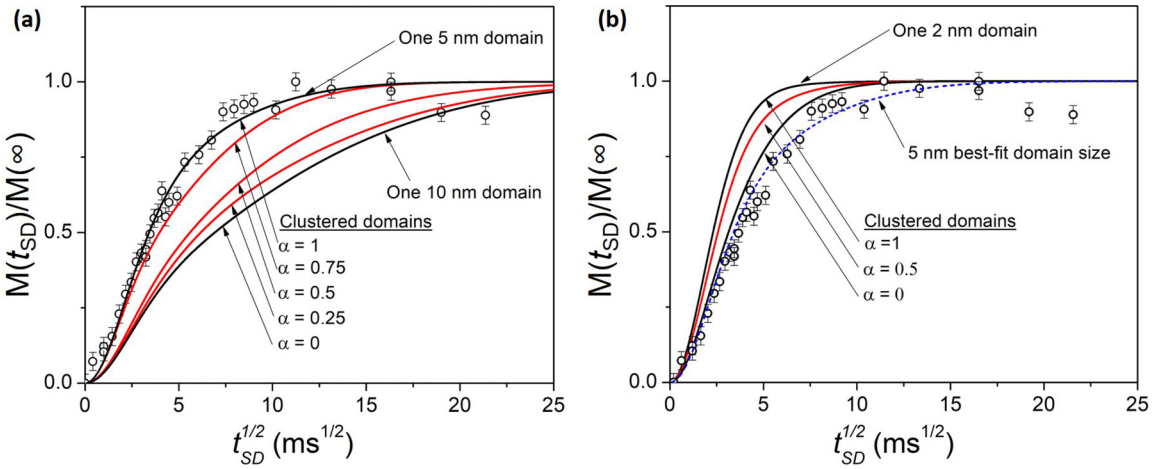

FIG. 6. (a) Simulated NMR spin magnetization recovery curves with normalized signal intensity $[M(t_{SD})/M(\infty)]$ for the clustered model in Fig. 4 as a function of α assuming an individual domain size of $d^{NMR} = 5$ nm. With increasing clustering, α decreases and the spin magnetization recovery curves approach equilibrium more gradually leading to an overestimation of the domain size. (b) Simulated NMR spin magnetization recovery curves assuming an individual domain size of $d^{NMR} = 2$ nm. The experimental results for the hydrated SDAPP membrane $S = 1.9$, $\lambda = 2.7$ (open symbols), plus the best fit $d^{NMR} = 5$ nm (blue dashed line) are also shown.

domains ($\alpha = 0$) to form a single large domain, the NMR spin magnetization recovery curve is indistinguishable from the recovery curve obtained from a 10-nm PPL structural model [Fig. 6(a)]. As disorder is introduced into the system in the form of domain clustering, the measured domain size from NMR spin diffusion is observed to increase, even though the sizes of the individual domains within the cluster remain constant. The analysis of the experimental NMR spin diffusion results for the hydrated SDAPP membrane in Fig. 6(a) illustrates two important results. First, using the simple 3D PPL structural model ($d^{NMR} = 5$ nm) provides an upper limit on the domain size, and the presence of clustering to produce a heterogeneous domain structure results in an overestimation of d^{NMR}. Second, the more extensive the degree of clustering the larger the impact on the estimated d^{NMR}. To further emphasize this point, Fig. 6(b) shows NMR spin diffusion simulations assuming a domain size of $d^{NMR} = 2$ nm. Again, with increasing clustering (decreasing α) the apparent domain size increases until the fully clustered limit of a single large domain (~4 nm) is reached. For this simple clustering model (Fig. 4) we find that the limiting domain size is given by

$$\lim_{\alpha \to 0} d^{NMR} \approx (N)^{1/\varepsilon} d_{domain}, \tag{12}$$

where ε is the dimensionality (i.e., 2D or 3D), N is the number of domains in the cluster, and d_{domain} is the size of the individual domains before clustering. Therefore, the NMR spin diffusion behavior in the presence of heterogeneous domain clustering is impacted by how close the individual hydrophilic domains are spatially located and by the number of smaller domains that may be incorporated into the effective cluster. Since the MD simulation for these SDAPP membranes predicts clustering of the hydrophilic domains, the fact that $d^{NMR} > d^*$ (Fig. 1) is no longer surprising because the NMR spin magnetization recovery curves are strongly impacted by the nonperiodic heterogeneous disordered nature of the polymer domains. Assuming an effective $d^{NMR} = 5$ nm with $N = 8$ and $\varepsilon = 3$, Eq. (12) estimates a 2.5-nm domain size (in the limit $\alpha = 0$) that now matches the $d^* \sim 2.5$ nm from SAXS, and the $d^* \sim 2.3$ nm from the MD simulation. The distribution in the size and the shape of the hydrophilic clusters as well as the heterogeneity in the local composition also impacts the width of the SAXS $S(q)$. While hydrophilic clustering may contribute to this heterogeneity, it is not the only factor controlling the widths in $S(q)$. A modified hard cylindrical model has been introduced to fit the width of the $S(q)$ ionomer peak for related materials [50].

IV. SUMMARY

Solid state NMR techniques such as NMR spin diffusion measurements are being widely applied to investigate the morphology and domain structure of heterogeneous polymers and materials. NMR spin diffusion experiments can be used to accurately measure domain sizes in systems containing ordered well-structured geometries, and many studies have found consistent domain sizes obtained from NMR spin diffusion and scattering techniques. However, the results presented here demonstrate that disorder and heterogeneity of polymer domain morphology can significantly influence the NMR spin diffusion measurements, yielding overestimation of effective domain sizes, an impact that is not readily appreciated. In cases where domain size distributions or heterogeneous domain clustering may exist, care must be taken when interpreting the NMR spin magnetization recovery curves with the knowledge that the domain size calculated assuming a simple 3D PPL structural model only provides an upper bound of dispersed domain size. For NMR spin diffusion techniques other structural input, either experimental or computational, needs to be incorporated into the development of structural models to improve the accuracy of the measured domain size. NMR spin diffusion experiments can then provide complimentary information to scattering experiments in testing and distinguishing different proposed structural models.

ACKNOWLEDGMENTS

This research was funded by the Sandia Laboratory Directed Research and Development (LDRD) program, with a portion of the work performed at the Center for Integrated Nanotechnologies, an Office of Science User Facility operated for the U.S. Department of Energy (DOE) Office of Science. Sandia National Laboratories is a multimission laboratory managed and operated by National Technology and Engineering Solutions of Sandia, LLC, a wholly owned subsidiary of Honeywell International, Inc., for the U.S. Department of Energy's National Nuclear Security Administration under Contract No. DE-NA-0003525. The views expressed in the article do not necessarily represent the views of the U.S. Department of Energy or the United States Government.

[1] M. Di Vona, D. Marani, A. D'Epifanio, S. Licoccia, I. Beurroies, R. Denoyel, and P. Knauth, J. Memb. Sci. **304**, 76 (2007).

[2] K. Miyatake, Y. Chikashige, E. Higuchi, and M. Watanabe, J. Am. Chem. Soc. **129**, 3879 (2007).

[3] Z. Wang, H. Ni, C. Zhao, M. Zhang, and H. Na, J. Appl. Polym. Sci. **112**, 858 (2009).

[4] J. K. Park, J. Li, G. M. Divoux, L. A. Madsen, and R. B. Moore, Macromolecules **44**, 5701 (2011).

[5] D. W. Shin, M. D. Guiver, and Y. M. Lee, Chem. Rev. **117**, 4759 (2017).

[6] T. Cheung, B. Gerstein, L. Ryan, R. Taylor, and D. Dybowski, J. Chem. Phys. **73**, 6059 (1980).

[7] J. Clauss, K. Schmidt-Rohr, and H. W. Spiess, Acta Polym. **44**, 1 (1993).

[8] D. E. Demco, A. Johansson, and J. Tegenfeldt, Solid State Nucl. Magn. Reson. **4**, 13 (1995).

[9] C. J. Garvey, I. H. Parker, G. P. Simon, and A. K. Whittaker, Holzforschung **60**, 409 (2006).

[10] D. Huster, X. Yao, and M. Hong, J. Am. Chem. Soc. **124**, 874 (2002).

[11] R. C. Nieuwendaal, H. W. Ro, D. S. Germack, R. J. Kline, M. F. Toney, C. K. Chan, A. Agrawal, D. Gundlach, D. L. VanderHart, and D. M. Delongchamp, Adv. Funct. Mater. **22**, 1255 (2012).

[12] D. VanderHart and G. McFadden, Solid State Nucl. Magn. Reson. **7**, 45 (1996).

[13] J. Wang, K. S. Jack, and A. L. Natansohn, J. Chem. Phys. **107**, 1016 (1997).

[14] B. R. Cherry, C. H. Fujimoto, C. J. Cornelius, and T. M. Alam, Macromolecules **38**, 1201 (2005).

[15] K. Schmidt-Rohr and H. Spiess, *Multidimensional Solid-State NMR and Polymers* (AP Inc., Mainz, Germany, 1994).

[16] K. S. Jack, A. Natansohn, J. Wang, B. D. Favis, and P. Cigana, Chem. Mater. **10**, 1301 (1998).

[17] K. S. Jack, J. Wang, A. Natansohn, and R. A. Register, Macromolecules **31**, 3282 (1998).

[18] E. G. Sorte, L. J. Abbott, A. L. Frischknecht, M. A. Wilson, and T. M. Alam, J. Polym. Sci. B. **56**, 62 (2017).

[19] T. Cheung, J. Phys. Chem. B **103**, 9423 (1999).

[20] H. Tanaka and T. Nishi, Phys. Rev. B **33**, 32 (1986).

[21] A. Buda, D. Demco, M. Bertmer, B. Blümich, V. Litvinov, and J. Penning, J. Phys. Chem. B **107**, 5357 (2003).

[22] K. Schäler, M. Roos, P. Micke, Y. Golitsyn, A. Seidlitz, T. Thurn-Albrecht, H. Schneider, G. Hempel, and K. Saalwächter, Solid State Nucl. Magn. Reson. **72**, 50 (2015).

[23] J. R. Havens and D. L. VanderHart, Macromolecules **18**, 1663 (1985).

[24] M. Mauri, Y. Thomann, H. Schneider, and K. Saalwächter, Solid State Nucl. Magn. Reson. **34**, 125 (2008).

[25] M. Roos, K. Schäler, A. Seidlitz, T. Thurn-Albrecht, and K. Saalwächter, Colloid. Polym. Sci. **292**, 1825 (2014).

[26] K. Saalwächter, Y. Thomann, A. Hasenhindl, and H. Schneider, Macromolecules **41**, 9187 (2008).

[27] E. G. Sorte, B. A. Paren, C. G. Rodriquez, Cy Fujimoto, C. Poirier, L. J. Abbott, N. A. Lynd, K. I. Winey, A. L. Frischknecht, and T. M. Alam, Macromolecules **52**, 857 (2019).

[28] T. J. Skalski, M. Adamski, B. Britton, E. M. Schibli, T. J. Peckham, T. Weissbach, T. Moshisuki, S. Lyonnard, B. J. Frisken, and S. Holdcroft, ChemSusChem **11**, 4033 (2018).

[29] L. J. Abbott and A. L. Frischknecht, Macromolecules **50**, 1184 (2017).

[30] Y. S. Yen and A. Pines, J. Chem. Phys. **78**, 3579 (1983).

[31] A. Buda, D. Demco, M. Bertmer, B. Blümich, B. Reining, H. Keul, and H. Höcker, Solid State Nucl. Magn. Reson. **24**, 39 (2003).

[32] A. Buda, D. Demco, B. Blümich, V. Litvinov, and J. Penning, ChemPhysChem **5**, 876 (2004).

[33] I. Schnell, Prog. Nucl. Magn. Reson. Spectrosc. **45**, 145 (2004).

[34] See Supplemental Material at http://link.aps.org/supplemental/10.1103/PhysRevMaterials.3.045602 for additional spin diffusion simulation, asymmetric distributions, and NMR DQ-filtered pulse sequences.

[35] M. Munowitz and A. Pines, in *Advanced Chemical Physics* (Wiley, New York, 2007), Vol. 66, pp. 1–152.

[36] M. Schneider, L. Gasper, D. Demco, and B. Blümich, J. Chem. Phys. **111**, 402 (1999).

[37] M. Voda, D. Demco, J. Perlo, R. Orza, and B. Blümich, J. Magn. Reson. **172**, 98 (2005).

[38] T. D. Gierke, G. E. Munn, and F. C. Wilson, J. Polym. Sci. Polym. Phys. Ed. **19**, 1687 (1981).

[39] K.-D. Kreuer, S. J. Paddison, E. Spohr, and M. Schuster, Chem. Rev **104**, 4637 (2004).

[40] B. Bae, K. Miyatake, and M. Watanabe, Macromolecules **42**, 1873 (2009).

[41] K. H. Lee, S. Y. Lee, D. W. Shin, C. Wang, S.-H. Ahn, K.-J. Lee, M. D. Guiver, and Y. M. Lee, Polymer **55**, 1317 (2014).

[42] X. Ma, C. Zhang, G. Xiao, D. Yan, and G. Sun, J. Polym. Sci.A **46**, 1758 (2008).

[43] Y. S. Kim, M. A. Hickner, L. Dong, B. S. Pivovar, and J. E. McGrath, J. Memb. Sci. **243**, 317 (2004).

[44] N. W. Ashcroft and N. D. Mermin, *Solid State Physics* (Holt, Rinehart and Winston, New York, 1976).
[45] G. Gebel, Polymer **41**, 5829 (2000).
[46] A. Kusoglu and A. Z. Weber, Chem. Rev. **117**, 987 (2017).
[47] T. Cheung, Appl. Spectrosc. **51**, 1703 (1997).
[48] K. Cooray and M. M. Ananda, Commun. Stat. Theory Methods **37**, 1323 (2008).
[49] A. Pewsey, Commun. Stat. Theory Methods **31**, 1045 (2002).
[50] C. F. Buitrago, D. S. Bolintineanu, M. E. Seitz, K. L. Opper, K. B. Wagener, M. J. Stevens, A. L. Frischknecht, and K. I. Winey, Macromolecules **48**, 1210 (2015).